

## Improving of the micro-turbine's centrifugal impeller performance by changing the blade angles

R. A. Tough<sup>1,2</sup>, A. M. Tousi<sup>2</sup>, J. Ghaffari<sup>2</sup>

### Summary

In this paper, micro-turbine centrifugal impeller with three different blade angles was investigated by using Computational Fluid Dynamics (CFD) method. The other basic geometric parameters are held constant. The influence of the blade angles change on the observed values was determined from numerical solution of the flow in the impeller with help of the FLUENT software. The numerical simulation focused on the air flow from compressor impeller inlet to exit, and the performance of impeller is predicted. The numerical solution was performed for original impeller geometry and for two other cases, in which blade inlet angle and backward sweep was changed. The standard  $k - \varepsilon$  turbulence model was used to obtain the eddy viscosity. Performance of the code was verified using measured data for the Eckardt impeller.

**Keywords:** micro-turbine centrifugal compressor, CFD, blade inlet angle, backward sweep

### Introduction

Microturbines are gas turbines with a power ranging approximately from 10 to 200 kW. These devices can be used in stationary, transport or auxiliary power applications. In a micro-turbine, a centrifugal compressor compresses the inlet air and a radial turbine change the hot gas kinetic energy to the rotary work. Both turbomachinery components are radial. Micro-turbine compressors have been widely accepted as effective devices to improve the performance of these engines. The flow through the centrifugal compressor is complex due to growth of boundary layers and flow separation on blade surfaces, the formation of secondary flows due to rotation and passage curvature and tip leakage in the impeller region. Resulting jet-wake formation is associated with high viscous losses and affects the operating range of the rotating impeller downstream. To improve the aerodynamic performance of centrifugal compressor it is necessary to suppress the separation and wake formation maintaining high level of diffusion within the impeller. It is essential to understand the flow structure to achieve these objectives within the passages. The complexity of the flow in a centrifugal impeller impacts the performance of impeller and makes it difficult to predict flow field correctly. Methods for accurate

---

<sup>1</sup>Corresponding author. E-mail address: reza\_tog@yahoo.com

<sup>2</sup>Department of Aerospace Engineering, Amir Kabir University of Technology, Tehran, Iran

prediction of turbulent flow in centrifugal impellers are important in order to get good estimate of the fluctuating loads in impeller.

Significant progress has been made in understanding impeller aerodynamic performance and also in predicting certain local flow details. The most popular guide to impeller design is diffusion parameter of some sort. Dean [1] discussed the influence of internal diffusion on impeller efficiency. His results, showed a trend of increasing efficiency with an increased overall diffusion ratio. Overall diffusion ratio is defined as the ratio of impeller inlet relative velocity, usually taken at the shroud, to impeller discharge relative velocity ( $w_1/w_2$ ). Kano et al. [2] presented results showing that in addition to the overall diffusion ratio, the rate of diffusion and maximum loading can significantly impact impeller peak efficiency and range. Moore et al. [3] used a three-dimensional viscous CFD method to examine the flow in a medium pressure ratio impeller. The CFD results showed several aspects of loss production in the impeller. Loss production was high over most of the shroud particularly within the clearance flow region. In most measurements of impeller efficiency, the inefficiency of the internal diffusion process is hidden by the large centrifugal pressure ratio. Detailed measurements of the internal flow made by Krain [5], Hathaway et al. [6], Skoch et al. [7], Kui Jiao et al. [8] and more recently Aghaei et al. [9] are helping to fill some gaps. Moreover, CFD has been widely recognized as a powerful method for predicting the performance and understanding the air flow characteristics of microturbine compressors, and has been widely used for numerical simulations in this area. Therefore, in this study, centrifugal impeller is investigated numerically by using the CFD method. The purpose of the present study is to investigate the feasibility of the performance improving of centrifugal compressor with respect to minimum changes only in impeller blade angles. Once a specific design is selected, then further numerical simulations with more stringent convergent criteria would be carried out before actually building the compressor and testing its performance. For this purpose, the impellers with three different blade angles are studied. Based on the simulation results, the flow characteristics for these different impellers are investigated and final model represented as improved model.

The flow calculation was carried out using a three-dimensional, finite volume, with a two-equation  $k - \epsilon$  turbulence model, for the solution of the time-averaged Navier-Stokes equations in a rotating frame of reference.

The performance of the code was verified using the measured data for the Eckardt backswept impeller. Eckardt (1976) performed detailed measurements in the high-speed backswept impeller.

### Impeller Definition

The impeller was designed to produce a stage pressure ratio of 4.2:1 at a corrected mass flow of 0.96 kg/s for a specific microturbine. The dimensionless specific speed is 0.60 with a blade corrected tip speed of 495 m/s. At the aerodynamic design point, the intent was to keep the impeller loading roughly constant along the flowpath while doing most of the internal diffusion over the first 30-50% of the impeller meridional chord. The overall diffusion ratio along the shroud surface was set at about 1.24 with the goal of achieving an 88% total to static efficiency for the stage.

The impeller consists of 12 blades with 30 degrees of backsweep from radial. A meridional cross-section of the flowpath is shown in Fig. 1 and some relevant geometric parameters are presented in Table 1.

Table 1: Some geometric parameters of impeller

Parameter	Unit	Amount
Inlet radius at tip ( $r_{1s}$ )	m	0.0548
Inlet radius at hub ( $r_{1h}$ )	m	0.0287
Outlet radius ( $r_2$ )	m	0.0952
Impeller exit width ( $b$ )	m	0.0032
Blade inlet angle ( $\beta_{1s}$ )	-	59
Blade backsweep ( $\beta_{B2}$ )	-	30

### Governing Equations

The conservation equations for mass, momentum and energy which govern the steady, viscous and compressible flow, expressed in a Cartesian coordinate system in a rotating frame of reference, are given as follows:

$$\frac{\partial}{\partial x_i} (\rho u_i) = 0 \quad \text{Mass} \quad (1)$$

$$\begin{aligned} \frac{\partial}{\partial x_i} (\rho u_i u_j) = & -\frac{\partial P}{\partial x_i} + \\ & \frac{\partial}{\partial x_i} \left[ \mu \left( \frac{\partial u_i}{\partial x_j} + \frac{\partial u_j}{\partial x_i} - \frac{2}{3} \frac{\partial u_k}{\partial x_k} \delta_{ij} \right) - \bar{\rho} \bar{u}'_i \bar{u}'_j \right] \\ & - 2\rho \varepsilon_{ijk} \Omega_{ijk} - \rho (\Omega_m x_m \Omega_i - \Omega_n \Omega_n x_i) \quad \text{Momentum} \quad (2) \end{aligned}$$

$$\begin{aligned} \frac{\partial}{\partial x_j} (\rho u_j H_R) = & \frac{\partial}{\partial x_j} (-q_j - \rho u'_j h') \\ & + \frac{\partial}{\partial x_j} \left[ u_i \left[ \mu \left( \frac{\partial u_i}{\partial x_j} + \frac{\partial u_j}{\partial x_i} - \frac{2}{3} \frac{\partial u_k}{\partial x_k} \delta_{ij} \right) - \bar{\rho} \bar{u}'_i \bar{u}'_j \right] \right] \quad \text{Energy} \quad (3) \end{aligned}$$

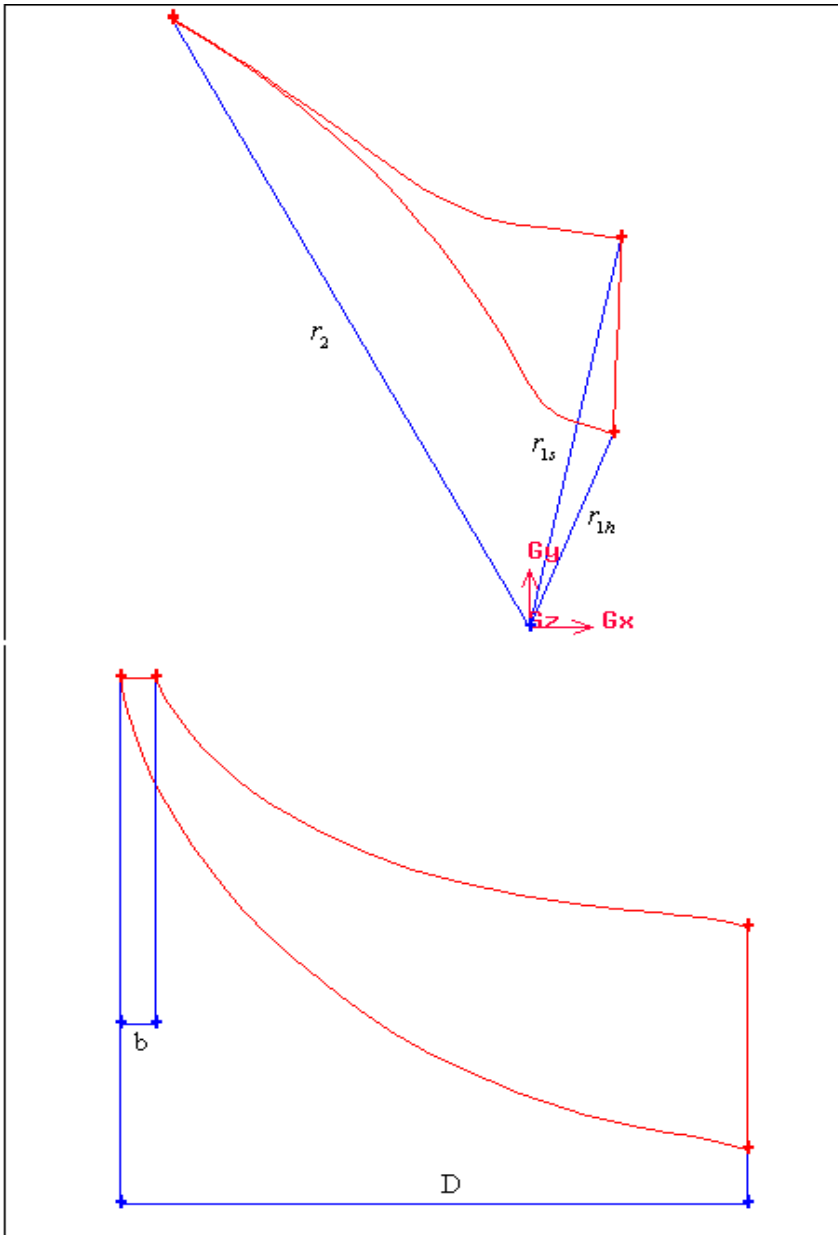


Figure 1: Illustration of impeller blade

Where  $H_R$  is rothalpy,  $\rho$  the density,  $\Omega$  the rotational speed, and  $\varepsilon_{ijk}$  the alternating tensor.

## Turbulence Modeling

Turbulence flows occur at high Reynolds numbers, when the inertia of the fluid overwhelms the viscosity of the fluid, causing the laminar flow motions to become unstable. Under these conditions, the flow is characterized rapid fluctuations in pressure and velocity which are inherently three dimensional and unsteady. It is an unfortunate fact that no single turbulence model is universally accepted as being superior for all classes of problems. The choice of turbulence model in turbo machinery will depend on considerations such as the physics encompassed in the flow, the established practice for a specific class of problem, the level of accuracy required, the available computational resources, and the amount of time available for the simulation. To make the most appropriate choice of model for your application, you need to understand the capabilities and limitations of the various options [9]. But, in turbo machinery problems, the usual methods are RSM and  $k - \varepsilon$ .

The conservation equations for the turbulence kinetic energy  $k$  and its rate of dissipation  $\varepsilon$  ( $m^2/s^3$ ) are shown in the following equations [10], [11]:

$$\frac{\partial}{\partial t}(\rho k) + \frac{\partial}{\partial x_i}(\rho k u_i) = \frac{\partial}{\partial x_j} \left[ \left( \mu + \frac{\mu_t}{\sigma_k} \right) \frac{\partial k}{\partial x_j} \right] + G_k - \rho \varepsilon - Y_M \quad (4)$$

$$\frac{\partial}{\partial t}(\rho \varepsilon) + \frac{\partial}{\partial x_i}(\rho \varepsilon u_i) = \frac{\partial}{\partial x_j} \left[ \left( \mu + \frac{\mu_t}{\sigma_\varepsilon} \right) \frac{\partial \varepsilon}{\partial x_j} \right] + C_{1\varepsilon} \frac{\varepsilon}{k} G_{kl} - C_{2\varepsilon} \rho \frac{\varepsilon^2}{k} \quad (5)$$

Where  $\sigma_k$  and  $\sigma_\varepsilon$  are the turbulent Prandtl numbers for  $k$  and  $\varepsilon$ , and constant values of 1.0 and 1.3 are used, respectively.  $G_k$  ( $kg/m^3 s^3$ ) represents the generation of turbulence kinetic energy due to the mean velocity gradients, and  $Y_M$  ( $kg/m^3 s^3$ ) is the contribution of the fluctuating dilatation in compressible turbulence to the overall dissipation rate, they are calculated as:

$$G_k = \left[ \mu_t \left( \frac{\partial u_i}{\partial x_j} + \frac{\partial u_j}{\partial x_i} \right) - \frac{2}{3} \left( \rho k + \mu_t \frac{\partial u_l}{\partial x_l} \right) \delta_{ij} \right] \frac{\partial u_j}{\partial x_i} \quad (6)$$

$$Y_M = 2\rho \varepsilon \frac{k}{\gamma RT} \quad (7)$$

Where  $\gamma$  and  $R$  are the specific heat ratio and gas constant ( $J/kgK$ ) of air, respectively, and  $T$  is temperature ( $K$ ).  $\mu_t$  is calculated as

$$\mu_t = C_\mu \rho \frac{k^2}{\varepsilon} \quad (8)$$

The values of the model constants  $C_{1\varepsilon}$ ,  $C_{2\varepsilon}$  and  $C_\mu$  are 1.44, 1.92 and 0.09, respectively.

## Numerical Simulation and CFD Analysis

Steady state conditions are simulated and air is assumed to be ideal gas for all the simulations. Since the current study only focuses on steady state simulations of the flow field, the results are considered valid only if the simulation is converged [8]. In this work, only one impeller channel was modeled for simulation. Using such an approach, the governing equations are solved in a reference frame that rotates at the rotational speed of the impeller. A similar method was used by Kui Jiao et al. [8], Aghaei et al. [9], Dickman, et al. [13], in their centrifugal compressor CFD simulations.

The CFD analysis was solved by means of FLUENT 6.2 software. The fully 3-D, compressible, viscous turbulent analysis of the fluid (air) flow was solved.

### Grid Generation

One of the most important and time-consuming tasks in the process of a CFD simulation is the generation of the computational grid. First of all is the decision whether the domain shall be discretized with hexahedral, tetrahedral or hybrid cells. Using tetrahedral cells can save a lot of time because the meshing of the volume works almost automatically. The grids for compressor channel were completely generated with the preprocessor GAMBIT 2 which offers some CAD tools as well as meshing tools. Three-Dimensional models of the impellers, that described above were generated. The channel domain (Fig. 2) had to be divided into several hexahedral volumes, each of which could be meshed with hexahedral cells.

To validate the numerical results, it is of great importance to check, whether the grid that has been used to discretize the computational domain complies with the requirements of the turbulence model used. One should also control some basic results of the computation, like Mach number or static pressure at prescribed locations in the domain, to check if they have different values using different grids.

The standard  $k - \varepsilon$  model ceases to be valid in the vicinity of walls, where the viscous stresses exceed the turbulent Reynolds-Stresses. To model the near-wall region a wall-function approach is used. The wall function does not actually resolve the flow in this region, but uses semi-empirical formulas to bridge the distance from the viscosity affected near wall region to the outer region, where turbulent stresses play the dominant role. This distance is measured in the dimensionless wall distance  $y^+$ . From experimental results the, law-of-the-wall is known to be valid in a range of about  $30 < y^+ < 60$  [14], [15]. The upper boundary depends among other on the Reynolds number, increasing with higher Re. Values of  $y^+ < 11.25$  should be avoided, because wall functions are not valid. Values of  $y^+ > 200$  should also be avoided, because the wake becomes substantially large above the log layer [3]. This indicates that the grid is too coarse and should be refined. Grid refinement

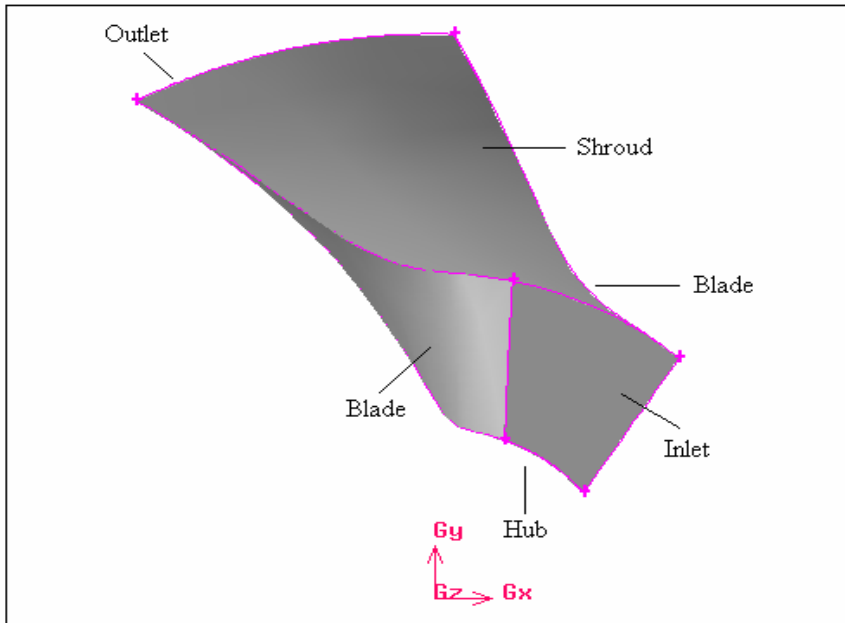


Figure 2: The one channel domain consisting of pressure and suction side of the main blade

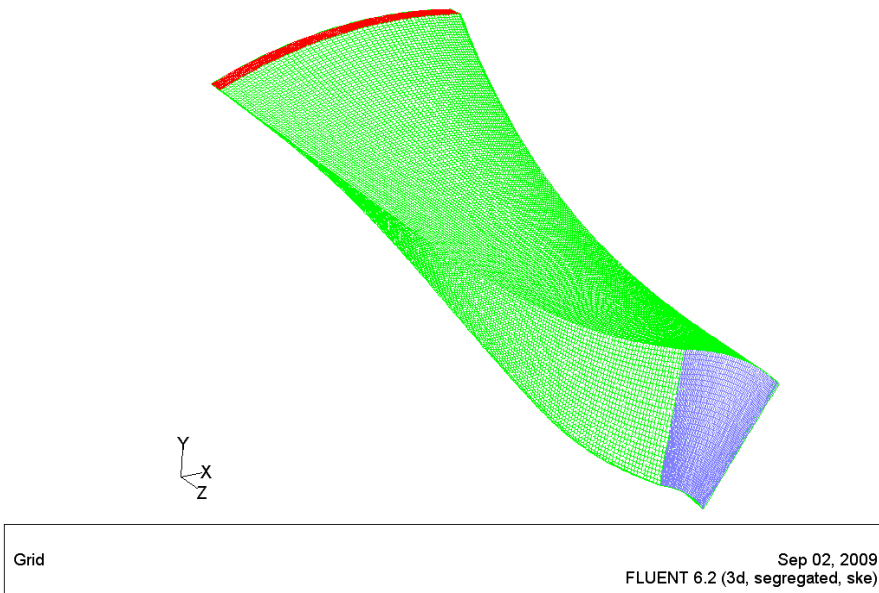


Figure 3: Computational mesh

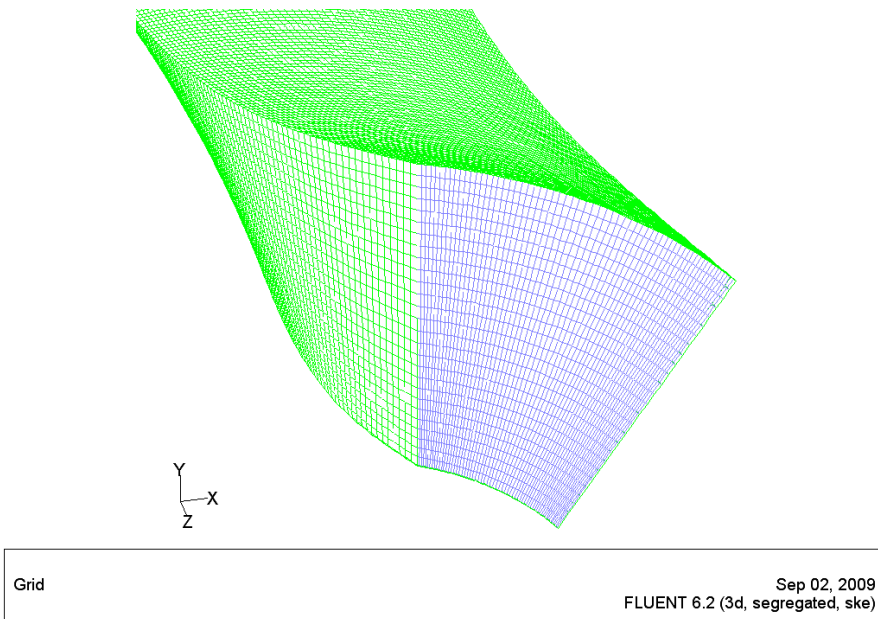


Figure 4: Computational mesh in inlet zone

can be performed by means of Grid adaptation using the obtained solution. For this work, near the solid walls, the standard wall function is used, and the range of  $y^+$  is between 25 and 80 which well accepted for the standard wall function [15].

To achieve consistent comparison, the total number of grid is about 314,000 for all the computational domains (numbers of grid for three different impellers). Grid dependency study is carried out locally refining the grids of the compressor. The total number of grid is increases up to 441,000 grids, about 40% more than the one shown in Fig. 3 and the difference in results (pressure, temperature, mass flow rate, etc.) for different grid system is less than 1.8% which is considered negligible. The details of the grid sensitivity and quality studies for final two grids are shown in Tables 2 and 3. This study shows that fine grid has some advantages.

### Boundary Conditions

The solution domain has one flow inlet and one flow outlet. Mass flow inlet boundary condition with atmosphere pressure and total temperature is specified for the impeller (channel) inlet. The turbulent kinetic energy is uniformly distributed with intensity of 10%. Pressure outlet boundary condition with a prescribed static pressure and backflow total temperature is used for the impeller outlet. The absolute velocities on the stationary shroud wall are equal to zero and the relative velocity on the blades and hub is zero. An adiabatic condition is imposed on the solid walls. Since the present study mainly focuses on steady state phenomena, the

Table 2: Grid sensitivity study

Parameter	Grid Case	Inlet	Outlet	Average $y^+$
Static Pressure (Pa)	1	85241.70	222277.43	32
	2	85108.30	222277.16	28
Total Pressure (Pa)	1	101343	435190.20	32
	2	101297.5	435371.70	28
Total Temperature (K)	1	288.78	457.51	32
	2	288.68	457.52	28
Absolute Vel. (m/s)	1	135.90	393.74	32
	2	136.30	394.60	28
Relative Vel. (m/s)	1	263.20	235.10	32
	2	263.70	235.20	28
Relative Mach Number	1	0.780	0.60	32
	2	0.781	0.60	28

Table 3: Comparison of two computational grid

Grid Property	Quantity			
	1-4	4-6	6-8	8-9
Aspect Ratio	89.79%	8.68%	1.45%	0.08%
Range	0.0-0.2	0.2-0.4	0.4-0.6	0.6-0.77
Equi Angle Skew	17.28%	72.80%	7.18%	2.74%

Multi-Reference Frame (MRF) [15] approach is used. Acceptable convergence was generally attained after 20,000 iterations.

### Validation

The aim of this validation is to check the reliability of present code to be used with confidence for the flow analysis. The data published by Eckardt (1976) [12] were chosen to validate the present code. Eckardt (1976) performed measurement for detailed investigation of flow field in a centrifugal impeller. The measured data have been widely used to validate computational codes and also quoted in describing the flow characteristics along the impeller.

The results of present calculation were compared with the measured data and the flow characteristics were also discussed in comparison with the given data. The geometry data were obtained from Eckardt (1976). The main geometric parameters of impeller are shown in Table 4.

The compressor operates at a rotational speed of 14,000 rpm and the design mass flow rate is 5.31 kg/s to produce a stage pressure ratio of 2.1. The inlet total pressure is 101.3 kPa and total temperature is 288 K [17]. Fig. 4 shows the Eckardt impeller's blade.

Table 4: Some geometric parameters of Eckardt impeller

Parameter	Unit	Amount
Blade numbers	-	20
Inlet radius at tip ( $r_{1s}$ )	m	0.14
Inlet radius at hub ( $r_{1h}$ )	m	0.045
Outlet radius ( $r_2$ )	m	0.20
Impeller exit width ( $b$ )	m	0.026
Blade inlet angle ( $\beta_{1s}$ )	deg	60
Blade backsweep ( $\beta_{B2}$ )	deg	0

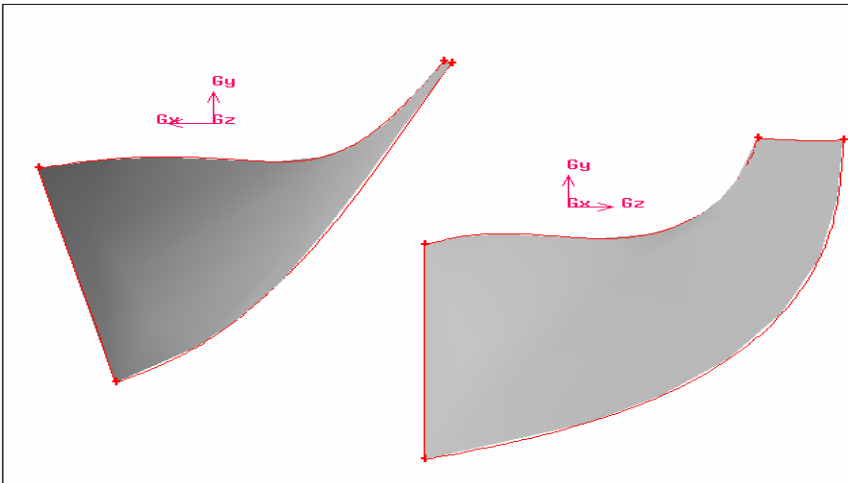


Figure 5: Eckardt impeller's blade

This impeller was analyzed at design speed for three mass flow rates and results were compared by experimental data.

The computation was carried out using fine mesh with 1,800,000 grids in calculation domain.

The overall performance parameters i.e. total pressure ratio ( $PR = 2.05$ ) and diffusion ratio ( $DR = 1.24$ ) are calculated and as example, total pressure ratio is shown in Fig.5. Calculated performance characteristics show good agreement with measurements. The predicted values of pressure ratio are 2% lower than the measured values at design conditions.

As seen above, the computational results agree reasonably well with the experimental results.

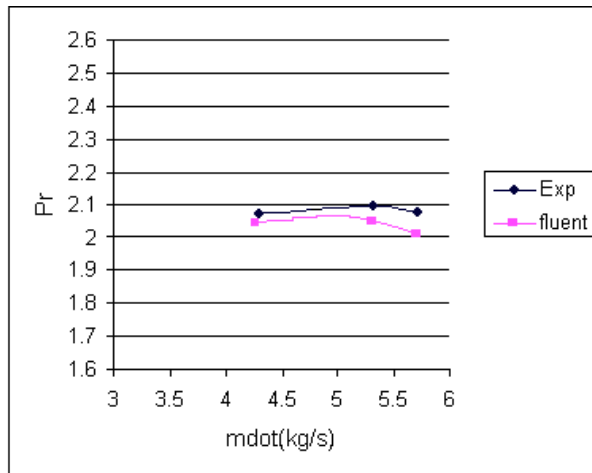


Figure 6: Calculated and experimental pressure ratio

### **Results of Numerical Solution of the Flow Field in the Original Impeller**

The fluid flow in the impeller was solved for the original blade. The calculated results using two fine grids are shown in table 5.

Table 5: Calculated results of original impeller simulation

Parameter	Grid	Inlet	Outlet
Static Pressure (Pa)	1	85241.71	222277.43
	2	85108.30	222277.16
Total Pressure (Pa)	1	101343.00	435190.20
	2	101297.50	435371.70
Total Temperature (K)	1	288.78	457.51
	2	288.68	457.52
Absolute Velocity (m/s)	1	135.90	393.74
	2	136.30	394.60
Relative Velocity (m/s)	1	263.20	235.10
	2	263.70	235.20
Relative Mach Number	1	0.780	0.60
	2	0.781	0.60

Base on these results, total pressure and diffusion ratios are 4.29 and 1.12 respectively.

Static pressure increase is linked to relative velocity drop, which is the reason to be especially concerned with these two quantities. The following figures show observed contours of flow field in channel.

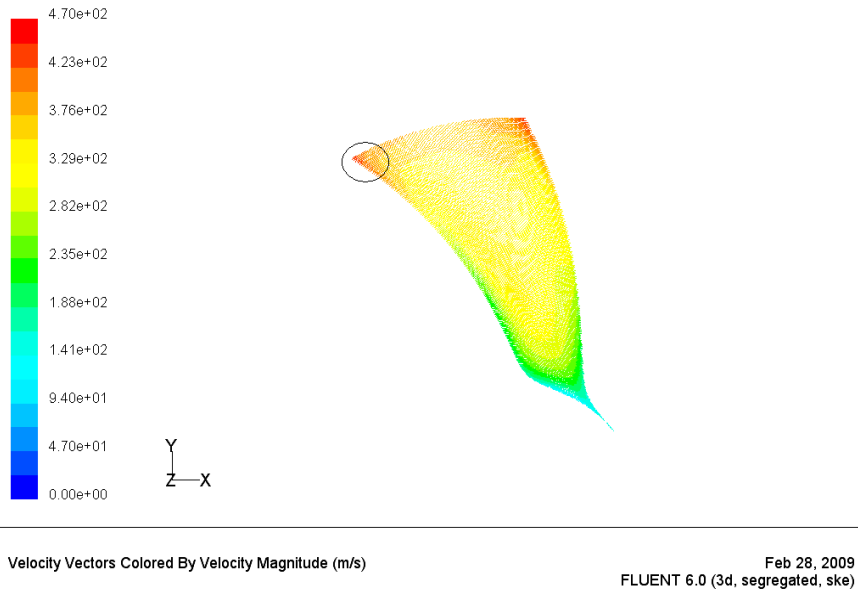


Figure 7: Absolute velocity contours

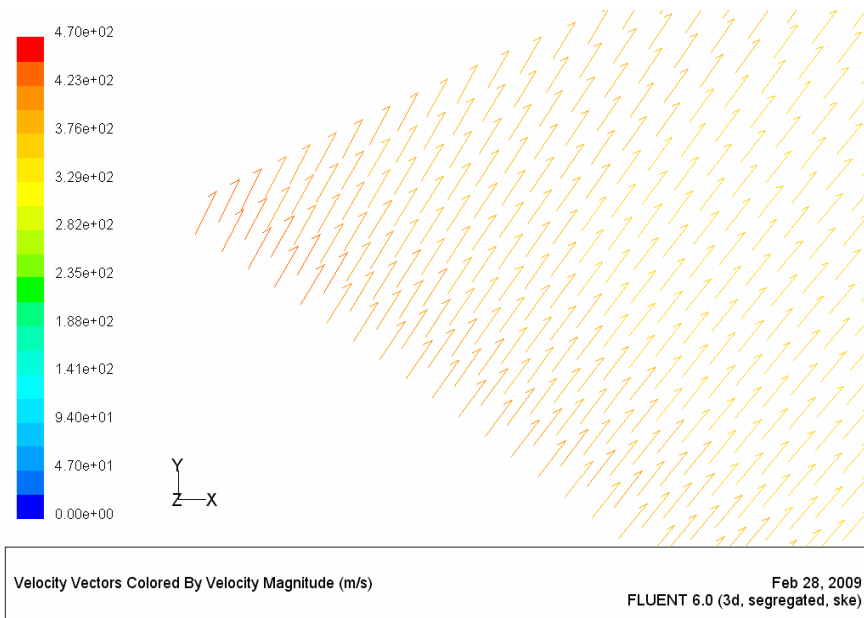


Figure 8: Absolute velocity vectors

The loss regions are shown in Fig. 9.

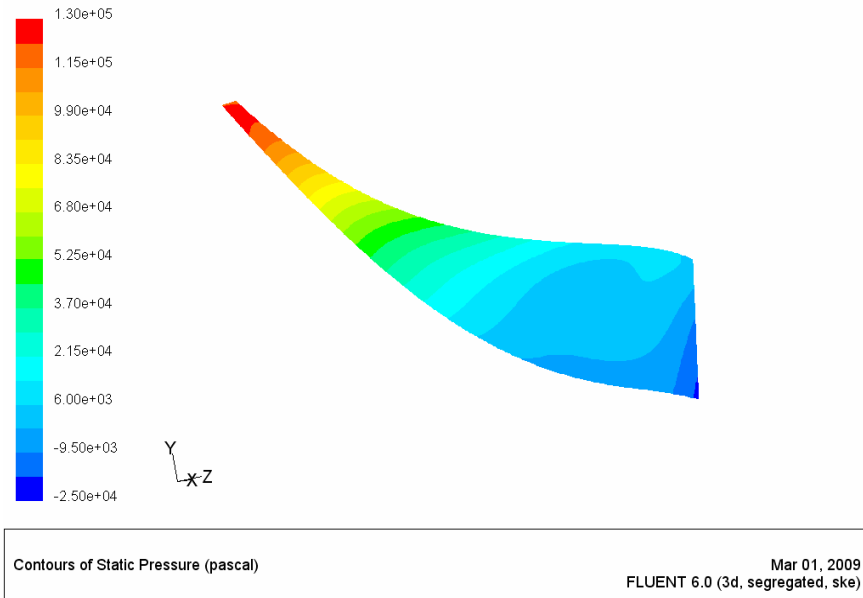


Figure 9: Static pressure contours

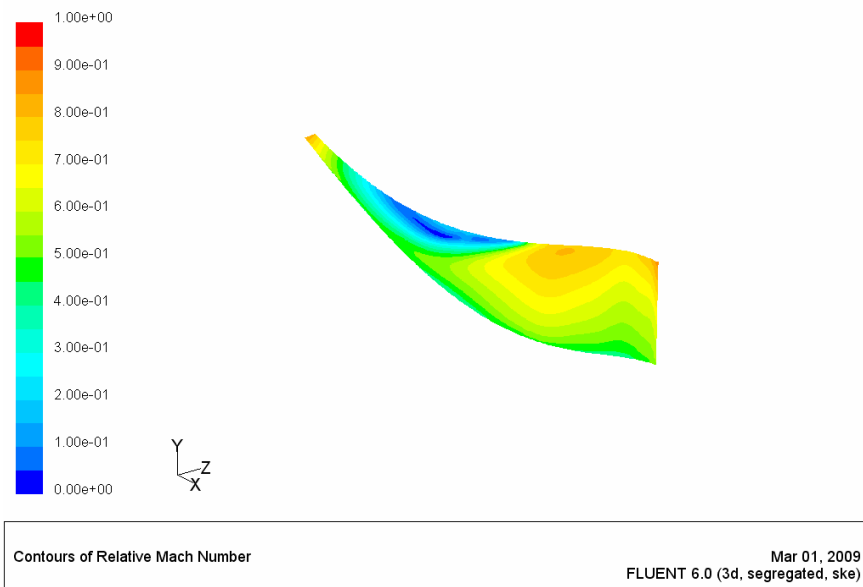


Figure 10: Relative Mach number contours (section: between suction and pressure surfaces)

As seen in Fig. 9, the rate of loss is increases as radius increase along passage. Moreover, high rotational speed and positive pressure gradient in comparison with Eckardt impeller cause to increase the loss region here.

### Case 2: Effects of Backward sweep Angle Decreasing on Impeller Performance

The blade backward sweep has significant effect on impeller flow physics. McCutcheon (1978) [16] during an optimization study observed that, aerodynamically, there is no optimum discharge blade angle and the blade backward sweep is limited by mechanical and physical limitations such tip speed, impeller diameter, the need to construct the blades with non-radial fibres, etc. In this work, we made changes in the impeller blade backward sweep angle, without any change in blade geometry and we observed the influence of this change on the loss distribution and impeller performance. This process was made in some steps and finally 3 degree of backward sweep was decreased. After this process, detailed CFD analysis of changed impeller was solved. Numerical analysis shows that the loss is decaying and pressure ratio and diffusion ratio is increasing with decreasing backward sweep angle. These improvements in performance parameters of impeller, led to increasing stage efficiency of compressor. The comparison between the original blade and changed blade is shown in the figure 10. It is important to mention that, the whole design of impeller was not changed through this process and we can use the same grid for CFD calculations.

The calculated results for changed impeller are shown in table 6.

Table 6: Calculated results for changed impeller simulation

Parameter	Inlet	Outlet
Static Pressure (Pa)	84947.10	224687.20
Total Pressure (Pa)	101325.50	455944.70
Total Temperature (K)	288.80	459.70
Absolute Velocity (m/s)	136.30	403.90
Relative Velocity (m/s)	268.50	233.00
Relative Mach Number	0.797	0.600

The pressure ratio and diffusion ratio for improved impeller is 4.4998 and 1.1524 respectively.

This noticeable rise in pressure ratio and diffusion ratio in comparison with original model is because of decreased loss region.

Fig. 11 shows the loss distribution within the channel as derived from the CFD results. In comparison with Fig. 9, it is clear that the loss region in changed impeller is small than original model.

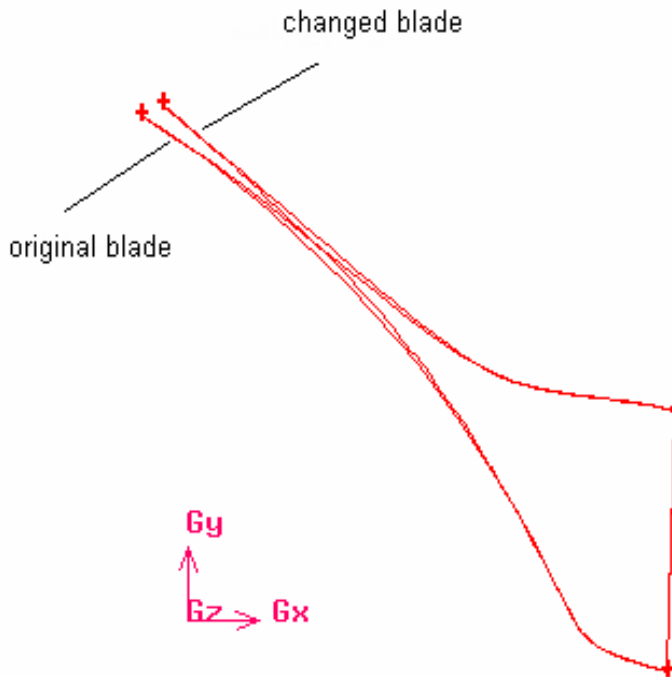


Figure 11: Comparison of original blade with changed blade

### Case 3: Effects of Increasing of Blade Inlet Angle on Impeller Performance

As above, the blade inlet angle was increased slightly at each step and finally 2 degree of increased inlet angle was accepted. After the final corrections on blade, the CFD analysis was done. It was found that increasing of blade inlet angle led to increase of pressure ratio and diffusion ratio. Clearly, increasing of pressure ratio can improve the stage efficiency of compressor. Again, it is important to memorize that this improvement in impeller performance is done without essential change in blade design.

Fig. 12 shows a comparison between original blade and changed blade's final shape.

The calculated results for changed impeller are shown in table 7.

The pressure ratio and diffusion ratio for improved impeller is 4.5997 and 1.165 respectively.

Increasing of pressure ratio is due to increasing of inlet momentum of flow and as seen in table 7, absolute velocity is larger than original one.

Figure 13 shows the loss distribution within the channel as derived from the CFD results. In comparison with Fig. 9, and Fig. 11 it is clear that the loss region

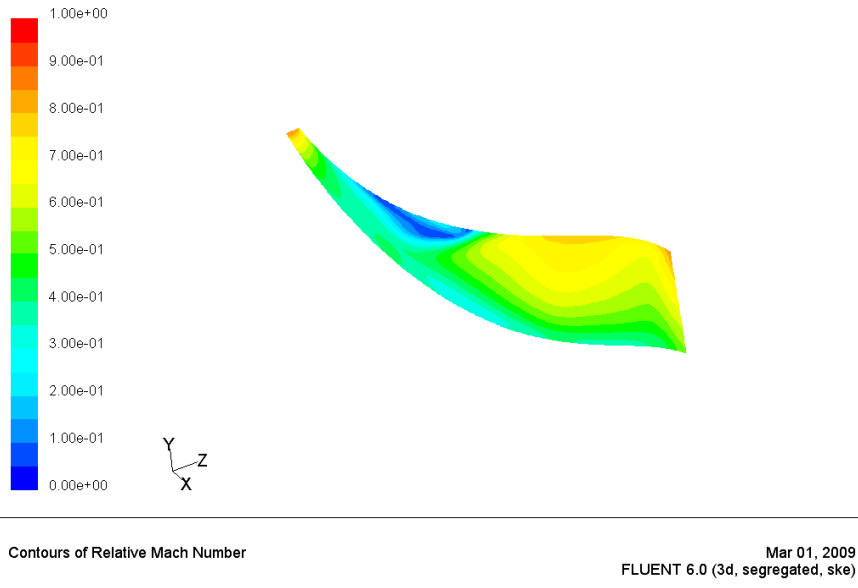


Figure 12: Relative Mach number contours (section: between suction and pressure surfaces)

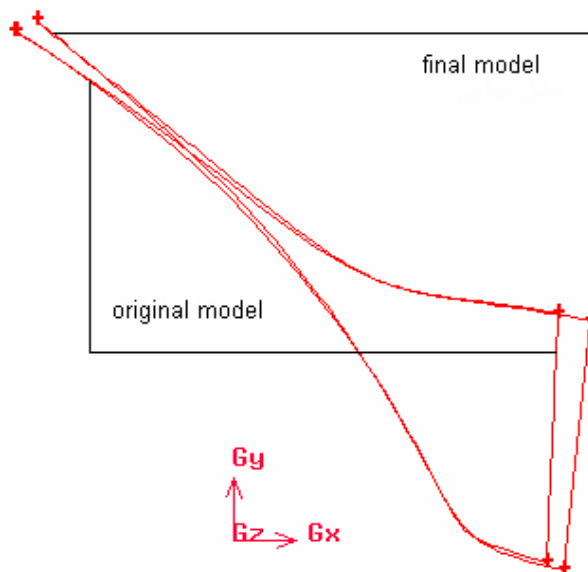


Figure 13: Comparison of original model with final model

Table 7: Calculated results for final model simulation

Parameter	Inlet	Outlet
Static Pressure (Pa)	83613.50	233607.80
Total Pressure (Pa)	101319.10	466036.30
Total Temperature (K)	288.30	461.50
Absolute Velocity (m/s)	140.50	406.20
Relative Velocity (m/s)	267.30	229.50
Relative Mach Number	0.797	0.580

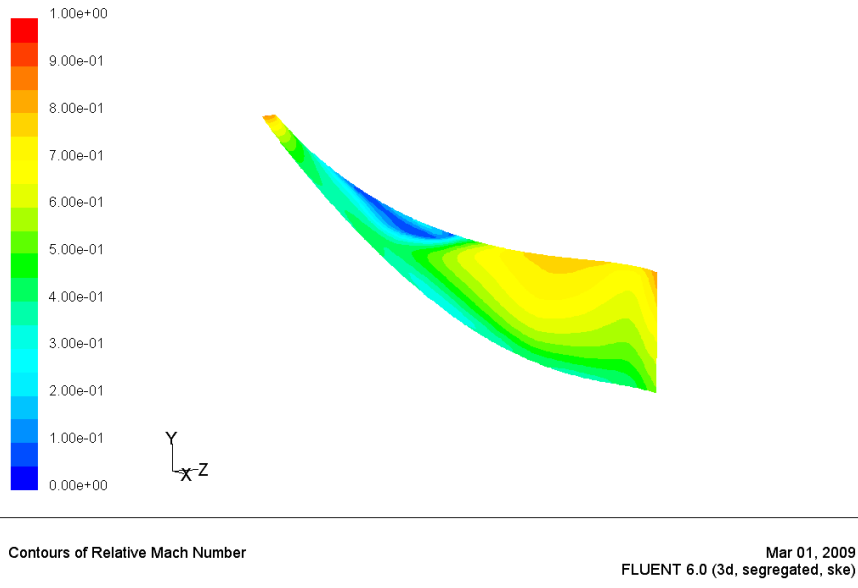


Figure 14: Relative Mach number contours (section: between suction and pressure surfaces)

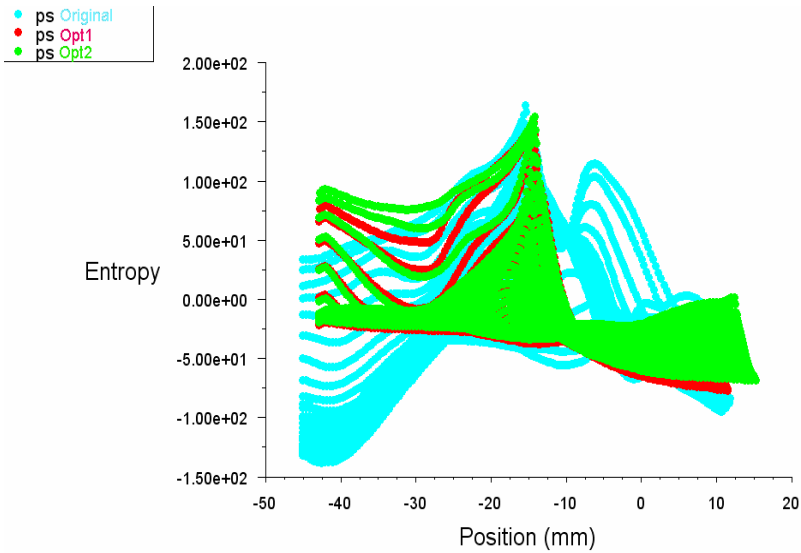
in Case 3 is small than other cases. As shown in Fig. 13 and table 7, the smallest loss region, highest pressure ratio and efficiency are all obtained in Case 3, which uses changed angles in blade inlet and backward sweep.

Figures 14 shows a comparison of development of the entropy field

$$(s = [1/(\gamma - 1)] \ln (p\rho^{-\gamma}))$$

on the pressure surface as derived from CFD results at the design flow operating condition. Figure 15 show a comparison between the entropy distributions on pressure surface for Original Case and Case 3.

Referring to figure 15, it can be observed that the high entropy region in Case 3 is very small than Original Case and entropy distribution is suitable in this case.



Entropy

Sep 16, 2009  
FLUENT 6.2 (3d, coupled imp, ske)

Figure 15: Comparing of the entropy distribution on pressure surface (Cyan: Original Case; Red: Case 2; Green: Case 3)

Close to the impeller mid region in Case 3, at 60% cord, the high entropy region is smallest than Original Case.

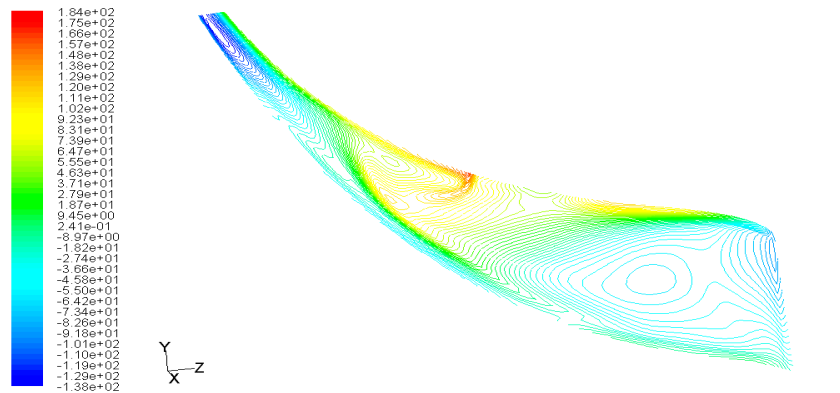
### Comparison of Final Results

Performance parameters of analyzed models in design condition are shown in table 8.

Table 8: Comparison of final results

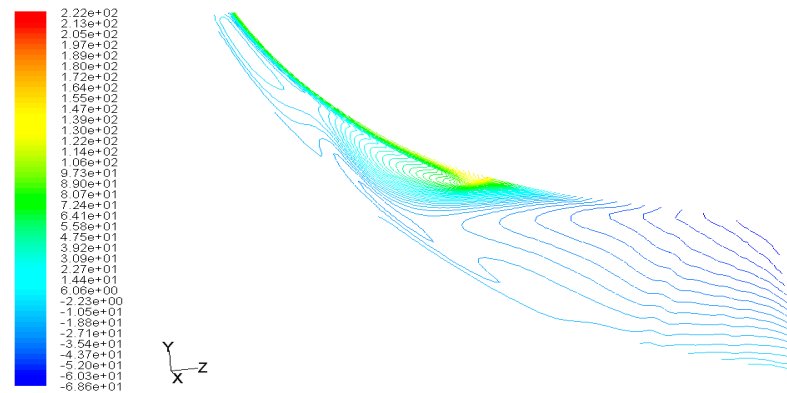
Model	Parameter			
	PR	DR	$\Delta T_0$	$\eta_C$
Original Case	4.2900	1.1200	168.70	0.880
Case 2	4.4998	1.1524	171.00	0.903
Case 3	4.5997	1.1650	173.00	0.908

Table 8 shows that changing the blade inlet and backward sweep has significant influence on impeller performance. Case 3 shows higher pressure and diffusion ratios and efficiency than Case 2 and Original Case. Based on the analysis of the flow characteristics of the 3 cases, the Case 3 becomes the most optimal design can be selected for centrifugal compressor of mentioned special microturbine. Case



Contours of Entropy

Sep 16, 2009  
FLUENT 6.2 (3d, coupled imp, ske)



Contours of Entropy

Sep 16, 2009  
FLUENT 6.2 (3d, segregated, ske)

Figure 16: Comparing of the entropy distribution on pressure surface (Up: Original Case; Down: Case 3)

3 combines the advantages of both decreasing of backward sweep and increasing of blade inlet angle, and it provide widest stable operating range and the highest pressure ratio and efficiency.

The main geometric parameters of final model of impeller are shown in Table 9.

### Conclusion

Steady state CFD simulations have been conducted in order to study the characteristics of different blade inlet angle and backward sweep. The calculations are performed on 3-D domains that reproduce the real geometry of the impeller to obtain

Table 9: Some geometric parameters of eckardt impeller

Parameter	Unit	Amount
Blade numbers	-	12
Inlet radius at tip ( $r_{1s}$ )	m	0.0548
Inlet radius at hub ( $r_{1h}$ )	m	0.0287
Outlet radius ( $r_2$ )	m	0.0952
Impeller exit width ( $b$ )	m	0.0032
Blade inlet angle ( $\beta_{1s}$ )	Deg	61
Blade backsweep ( $\beta_{B2}$ )	deg	27

the rotational speed of 50,000 rpm. Corresponding to different blade angles, three cases are studied, and the analysis of the flow characteristics is also performed to obtain a better understanding of the influence of blade angles on impeller behaviors. The present code correctly predicts the pressure ratio, diffusion ratio and efficiency of the centrifugal impeller. The predicted flow development through the impeller is in good agreement with the measured data. The code reasonably simulates the loss region which affects the stage efficiency of compressor. The distribution of loss is strongly three dimensional and correlated with the blade angles. It was found that 3 degree reduction in backward sweep and 2 degree increase in blade inlet angle could have a wider stable operating range and higher pressure, diffusion ratios and efficiency by comparing with its corresponding original blade. This is because of the small loss region in channel passage and prevention of the flow separation due to increased momentum of flow in impeller inlet.

### References

1. L.M.Larosillere, G.J.Skoch, "Aerodynamic Synthesis of a Centrifugal Impeller Using CFD and Measurements", NASA Tech. Memorandum 107515, 1997.
2. M. Zangeneh, "Inviscid-Viscous Interaction method for Three Dimensional Invers Design of Centrifugal Impellers", UCL, London, Trans of ASME Journal of Turbomachinery 116:280-290, 1994
3. M. Zangeneh, "A Compressible Three Dimensional Blade Design Method for Radial and Mixed Flow Turbomachinery Blades", Int. J. Numerical Methods in Fluids 13:599-624, 1991.
4. Liu Zhengxian et al., "Computational and Experimental Investigation of 3-D Turbulent Flow Field in Centrifugal Impeller. Fluidmachinery" 28(4):9-12, 2000.
5. Hah C, Wennerstorm AJ, "Three Dimensional Flow Fields inside a Transonic compressor With Swept Blades", Journal of Turbomachinery 113:241-250,

- 1991.
6. Hillewaert K, Van den Braembussche RA, "Numerical Simulation of Impeller-Volute Interaction in Centrifugal Compressors. *Journal of Turbomachinery*", 121(3):603-608, 1999.
  7. Tan Dazhi, Yuan Xin, "Application of Higher-Order High Resolution Scheme for Turbulence Flow in Centrifugal Impeller Passage", *Turbine Technology* 45(3):139-141, 2003.
  8. Jiao K et al. "Numerical Simulation of Air Flow through Turbocharger Compressors With dual Volute Design", *Appl Energy* (2009), doi:10.1016/j.apenergy.2009.02.019
  9. Aghaei tog R., Tousei A. M., Tourani A., "Comparison of Turbulence Methods in CFD Analysis of Compressible Flows in Radial Turbomachines", *Journal of Aircraft Engineering and Aerospace Technology*, Emerald, London, 2008, Vol.180, Issue 6.
  10. Aghaei tog R., Tousei A. M., "1D Design and 3D CFD Analysis of the Flow Field in Centrifugal Turbomachines", ICCES05, IT Madras, Chennai, India, 2005.
  11. Aghaei tog R., Tousei A. M., "Design and CFD Analysis of Centrifugal Compressor for a Microgasturbine", *Journal of Aircraft Engineering and Aerospace Technology*, Emerald, London, Vol 79/ 2/07 issue (March/April 07), 2007.
  12. D. Eckardt, "Detailed Flow Investigations Within a High-Speed Centrifugal Compressor Impeller", *Trans. ASME*, September, 1976.
  13. H.P. Dickmann, T.S. Wimmel, J. Szwedowicz, D. Filsinger, C.H. Roduner, "Unsteady Flow in a Turbocharger Centrifugal Compressor: Three-Dimensional Computational Fluid Dynamics Simulation and Numerical and Experimental Analysis of Impeller Blade Vibration", *J Turbomach* 2006;128:455-65.
  14. Tamm A, Gurge M., Stoffel B. "Experimental and 3-D Numerical Analysis of the Flow Field in Turbomachines Part Two" Darmstadt University of Technology, 1999.
  15. *Fluent5 User's Guide*, FLUENT Inc. 1998.
  16. Mc Cutcheon A R S (1978), "Aerodynamic Design and Development of a High Pressure Ratio Turbocharger Compressor", *IME paper C73/78*, 1978.
  17. Zhang Li, Chen Hanping, Xu Zhong, "A Quasi-3D Numerical Analysis of a Centrifugal Compressor Impeller", *Fan Technology* 5:3-7, 2000.

18. Japikse, D., "Assessment of single and two-zone modeling of centrifugal compressors. Studies in component performance: Part 3", ASME Paper No. 85-GT-73, 1985.